J. Fluid Mech. (1979), *vol.* 94, *part* 2, *pp.* 305–330
Printed in Great Britain

The generation of feeding currents by flagellar motions

By J. J. L. HIGDON

Department of Applied Mathematics and Theoretical Physics, University of Cambridge†

(Received 14 December 1978)

The use of flagella by sessile organisms to generate feeding currents is analysed. The organism consists of a spherical cell body (radius A) to which a smooth flagellum (radius a, length L) is attached radially. The cell body is a height H above the plane substrate to which it is rigidly attached via a stalk. The organism propagates plane sinusoidal waves (amplitude α, wavenumber k) from base to tip. The flagellum is represented by distributions of stokeslets and dipoles along its centre-line. The cell body and substrate are modelled by employing an approximate form of the Green's function for the sphere in the half space. The error terms in the model are $O(a/L)$ and $O(A^2/H^2)$. The analysis and method of solution are adapted from Higdon (1979).

The mean flow rate and power consumption are calculated for a wide range of parameters. Optimal motions are determined with the criterion of minimizing the power required to achieve a given flow rate. The optimum wave has maximum slope in the range $2 < \alpha k < 2{\cdot}5$ (compared to the optimum value $\alpha k = 1$ for swimming). The optimum number of waves N_λ increases linearly with flagellar length for $L/A > 10$ and is approximately constant, $N_\lambda = 1$, for shorter flagella. The optimum flagellar length is in the range $5 < L/A < 10$. There is no optimum flagellar radius a/A. For optimal efficiency, the height H should be greater than or equal to the length of the flagellum.

The optimum values of the parameters are compared to the values for the choanoflagellates described by Lapage (1925) and Sleigh (1964). Excellent agreement is found between the predicted optima and the observed values. The calculated velocity field closely resembles the flow described by Sleigh and Lapage.

1. Introduction

Micro-organisms which utilize flagellar motions have been the subject of considerable study by hydrodynamicists. In the past, these studies have concentrated on the locomotion of organisms by flagellar propulsion. In this paper, we consider a quite different application: the use of flagella by sessile organisms to generate feeding currents. As there is a wide variety of shapes, sizes and flagella among these organisms, it is necessary to restrict the present effort to a single class of organisms, the 'choanoflagellates' or collar flagellates. These organisms attach themselves to the substrate via a long stalk and propagate plane waves down a smooth flagellum to produce the desired flow field. The organism ingests food by filtering the stream which passes through a collar surrounding the base of the flagellum. Typically, this collar is composed of a large number of fine filaments called pseudopodia.

† Present address: Department of Chemical Engineering, Stanford University, California 94305.

0022–1120/79/4293–7290 $02.00

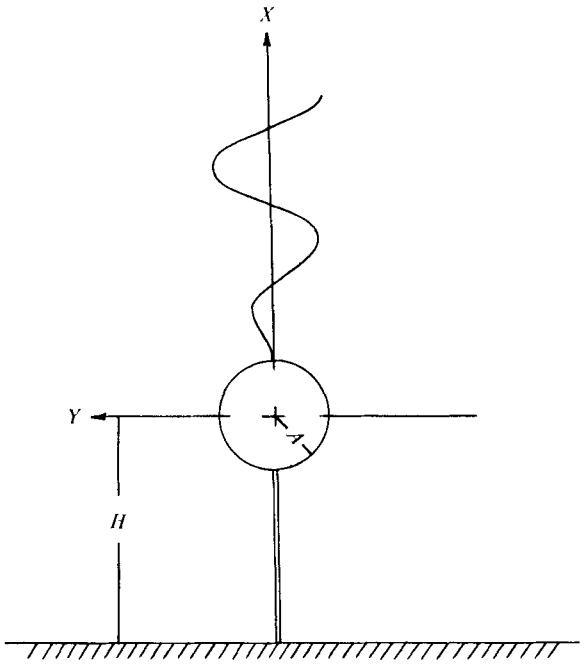

FIGURE 1. Example of a sessile organism showing relative position of cell body, flagellum and plane substrate.

A general overview of the feeding processes of flagellates is given in Sleigh (1973), chapter 5. Lapage (1925) gives a detailed description of a typical collar flagellate and the flow field it generates. For a description of the flagellar activity of a variety of sessile organisms see Sleigh (1964).

The study of these flow fields from a mathematical viewpoint has been extremely limited. Lunec (1975) modelled an isolated flagellum using force coefficients and calculated the velocity field in the vicinity of the flagellum. A comparison with the flow about an actual organism demonstrated the need to adopt a more sophisticated model to account for the interaction of the flagellum with the cell body and other boundaries. Lighthill (1976) presented a semi-quantitative theory which outlines the role of the flagellum in generating the flow field and its dependence on the parameters.

The representation of the organism employed in this paper is shown in figure 1. The filaments which compose the collar of the organism are extremely fine and do not actively affect the flow; hence it is assumed that they may be ignored. The cell body is treated as a sphere of radius A to which a single smooth flagellum of radius a and length L is attached radially. The flagellum propagates plane sinusoidal waves from base to tip. The cell body is a distance H above the substrate, to which it is rigidly attached via a stalk. As it is motionless, the stalk has a much smaller effect on the flow than the flagellum and is ignored. The substrate is represented as a smooth plane surface extending to infinity.

The characteristic length of the organism is 10 μm and the Reynolds' number is of order 10^{-4}. The flow is governed by Stokes' equations. The analysis follows the method used by Higdon (1979, hereafter referred to as I) in studying flagellar propul-

sion. In that paper, slender body theory was used to show that the flagellum may be represented by distributions of stokeslets and dipoles along its centre-line. The presence of the spherical cell body and the plane substrate are accounted for by employing the Green's function for the flow external to a sphere in the half space. An approximate expression for this Green's function is constructed from the individual Green's functions via the method of reflexions. The errors in the analysis are $O(a/L)$ for the slender body theory and $O(A^2/H^2)$ for the approximate Green's function.

The use of slender body theory and the Green's function transforms the problem into a pair of singular integral equations for the force distributions along the flagellum. As in I, these equations are solved by an iteration process. The solution for the force distribution is then employed to find the velocity field and the power consumption. The parameters for the organism and the wave form are varied to find the optimal configuration with the criterion of minimizing the power consumption for a given flow rate.

2. Singularity solutions of Stokes' equations

The fundamental singularity solution of Stokes' equations is called a stokeslet and is defined by

$$S_{jk}(\mathbf{x}, \mathbf{y}) = \delta_{jk}/r + (x_j - y_j)(x_k - y_k)/r^3, \tag{1}$$

where $r = |\mathbf{x} - \mathbf{y}|$.

The velocity at $\mathbf{x}$ due to a stokeslet of strength $\mathbf{f}$ at $\mathbf{y}$ is

$$u_j(\mathbf{x}) = S_{jk}(\mathbf{x}, \mathbf{y}) \frac{f_k}{8\pi\mu}. \tag{2}$$

Physically, this represents the velocity field due to a point force $\mathbf{f}$ in an unbounded fluid. Mathematically, the stokeslet is the free space Green's function for Stokes' equations. This means that the solution of Stokes' equations may be expressed in terms of stokeslets and their normal derivatives over the boundaries.

Any derivative of a stokeslet is a solution of Stokes' equations. This follows immediately from the linearity of the equations. Thus, it is possible to obtain singularity solutions of any order by taking the appropriate derivative of the stokeslet. The gradient of a stokeslet is called a Stokes-doublet. To obtain the Stokes-doublet in its standard form, differentiate (1) with the operator $\partial/\partial y_l$:

$$S_{D_{jkl}}(\mathbf{x}, \mathbf{y}) = \left(\frac{-\delta_{kl}}{r^3} + \frac{3(x_k - y_k)(x_l - y_l)}{r^5}\right)(x_j - y_j) + \left(\frac{(x_l - y_l)\delta_{jk} - (x_k - y_k)\delta_{jl}}{r^3}\right). \tag{3}$$

The Stokes-doublet has tensorial strength σ_{kl}. The velocity due to a Stokes-doublet σ_{kl} at the point $\mathbf{y}$ is

$$u_j(\mathbf{x}) = S_{D_{jkl}}(\mathbf{x}, \mathbf{y}) \frac{\sigma_{kl}}{8\pi\mu}. \tag{4}$$

The symmetric component of the Stokes-doublet, represented by the first bracket in (3), is called a stresslet. The antisymmetric component, represented by the second bracket in (3), is called a rotlet. The rotlet represents the velocity field due to a point torque.

Among the singularities obtained by taking the second derivative of the stokeslet,

the most useful is the potential dipole, defined by the Laplacian of the stokeslet. To obtain the dipole in its standard form, differentiate (1) with the operator $-\frac{1}{2}\nabla_y^2$:

$$D_{jk}(\mathbf{x},\mathbf{y}) = \frac{-\delta_{jk}}{r^3} + \frac{3(x_j-y_j)(x_k-y_k)}{r^5}. \tag{5}$$

The velocity field for a dipole of strength $\mathbf{d}$ at $\mathbf{y}$ is

$$u_j(\mathbf{x}) = D_{jk}(\mathbf{x},\mathbf{y})\frac{d_k}{4\pi}. \tag{6}$$

These three singularities, stokeslet, Stokes-doublet and dipole, are the most useful singularities in constructing solutions to Stokes' equations.

3. Image system for a sphere

In some problems with special geometry, it is possible to find combinations of singularities which simplify the solution of the equations by satisfying the boundary condition implicitly. The set of singularities in such a case includes the stokeslet, as the fundamental solution, plus a collection of image singularities located within the boundary, which serve to cancel the velocity of the stokeslet on the boundary. The stokeslet plus its images provides an expression for the Green's function for Stokes' equations in the region confined by the boundary.

The Green's function for the flow external to a sphere is

$$G_{S_{jk}}(\mathbf{x},\mathbf{y}) = S_{jk}(\mathbf{x},\mathbf{y}) + S^*_{jk}(\mathbf{x},\mathbf{y}), \tag{7}$$

where S^*_{jk} represents the image system.

The velocity at the point $\mathbf{x}$ due to a point force $\mathbf{f}$ at the point $\mathbf{y}$ in the presence of a sphere is given by

$$u_j(\mathbf{x}) = G_{S_{jk}}(\mathbf{x},\mathbf{y})\frac{f_k}{8\pi\mu}. \tag{8}$$

Oseen (1927) gives the expression for S^*_{jk} when the sphere has its centre at the origin:

$$\begin{aligned} S^*_{jk}(\mathbf{x},\mathbf{y}) = {} & -\frac{A}{|\mathbf{y}|}\frac{\delta_{jk}}{r^*} - \frac{A^3}{|\mathbf{y}|^3}\frac{(x_j-y_j^*)(x_k-y_k^*)}{r^{*3}} - \frac{|\mathbf{y}|^2-A^2}{|\mathbf{y}|^2}\left\{\frac{y_j^*y_k^*}{A^3r^*} - \frac{A}{|\mathbf{y}|^2r^{*3}}\right. \\ & \left.\times[y_j^*(x_k-y_k^*)+y_k^*(x_j-y_j^*)] + \frac{2y_j^*y_k^*}{A^3}\frac{y_l^*(x_l-y_l^*)}{r^{*3}}\right\} - (|\mathbf{x}|^2-A^2)\frac{\partial\phi_k}{\partial x_j}; \end{aligned} \tag{9}$$

$$\begin{aligned} \frac{\partial\phi_k}{\partial x_j} = {} & \frac{|\mathbf{y}|^2-A^2}{2|\mathbf{y}|^2}\left\{-\frac{3y_k(x_j-y_j^*)}{Ar^{*3}} + \frac{A\delta_{jk}}{r^{*3}} - 3A\frac{(x_j-y_j^*)(x_k-y_k^*)}{r^{*5}}\right. \\ & -\frac{2y_ky_j^*}{Ar^{*3}} + \frac{6y_k}{Ar^{*5}}(x_j-y_j^*)(x_l-y_l^*)y_l^* \\ & + \frac{3A}{|\mathbf{y}^*|}\frac{y_k^*(x_j-y_j^*)r^{*2} + (x_j-y_j^*)(x_k-y_k^*)|\mathbf{y}^*|^2 + (r^*-|\mathbf{y}^*|)r^{*2}|\mathbf{y}^*|\delta_{jk}}{r^{*3}|\mathbf{y}^*|(|\mathbf{y}^*|+x_iy_i^*-|\mathbf{y}^*|^2)} \\ & - \frac{3A}{|\mathbf{y}^*|}\frac{(|\mathbf{y}^*|(x_j-y_j^*)+r^*y_j^*)(y_k^*r^{*2}-(x_k-y_k^*)|\mathbf{y}^*|^2+(x_k-2y_k^*)r^*|\mathbf{y}^*|)}{r^{*2}|\mathbf{y}^*|(|\mathbf{y}^*|r^*+x_iy_i^*-|\mathbf{y}^*|^2)^2} \\ & \left. - \frac{3A}{|\mathbf{y}^*|}\frac{x_jy_k^*+|\mathbf{x}|\,|\mathbf{y}^*|\delta_{jk}}{|\mathbf{x}|\,|\mathbf{y}^*|(|\mathbf{x}|\,|\mathbf{y}^*|+x_iy_i^*)} + \frac{3A}{|\mathbf{y}^*|}\frac{(|\mathbf{y}^*|x_j+|\mathbf{x}|y_j^*)(|\mathbf{y}^*|x_k+|\mathbf{x}|y_k^*)}{|\mathbf{x}|\,|\mathbf{y}^*|(|\mathbf{x}|\,|\mathbf{y}^*|+x_iy_i^*)^2}\right\}; \end{aligned} \tag{10}$$

where A is the radius of the sphere, $\mathbf{y}^*$ is the inverse point defined by

$$\mathbf{y}^* = \frac{A^2}{|\mathbf{y}|^2}\mathbf{y} \tag{11}$$

and $r^* = |\mathbf{x}-\mathbf{y}^*|$.

The expression for S^*_{jk} is quite complicated. It can be more easily understood in terms of the components of the stokeslet. For the radial component of the stokeslet, the images are a stokeslet, dipole and stresslet at the inverse point. For the transverse component, the images are a line distribution of stokeslets, dipoles and Stokes-doublets extending from the origin to the inverse point.

The total stokeslet strength and rotlet strength give the force and moment on the sphere.

The force and moment for the radial component are

$$\mathbf{F} = \left(-\frac{3}{2}\frac{A}{|\mathbf{y}|}+\frac{1}{2}\frac{A^3}{|\mathbf{y}|^3}\right)\mathbf{f}_r, \quad \mathbf{M} = 0. \tag{12}$$

For the transverse component

$$\mathbf{F} = \left(-\frac{3}{4}\frac{A}{|\mathbf{y}|}+\frac{1}{4}\frac{A^3}{|\mathbf{y}|^3}\right)\mathbf{f}_t, \quad \mathbf{M} = -\frac{A^3}{|\mathbf{y}|^3}\mathbf{y}\times\mathbf{f}_t. \tag{13}$$

Consider now the problem of finding images for higher-order singularities. The function $G_{S_{jk}}$ defined by (7) has the property that $G_{S_{jk}} = 0$ for $|\mathbf{x}| = A$ independent of $\mathbf{y}$. Thus, $D_y G_{S_{jk}} = 0$ on $|\mathbf{x}| = A$ for any differential operator D_y with respect to the variable $\mathbf{y}$. It is important here to distinguish between the free variable $\mathbf{x}$ and the parametric variable $\mathbf{y}$.

From this property of $G_{S_{jk}}$, the following rule may be formulated.

If a solution of Stokes' equations is defined by $D_y S_{jk}$ for a differential operator D_y, the image system in the sphere for the singularity is $D_y S^*_{jk}$.

This rule gives a method for finding the images of the Stokes-doublet and dipole. In practice, the differentiation of (9) is very difficult. To obtain an approximate expression for S^*_{jk} which will be easily differentiable with respect to $\mathbf{y}$, consider an expansion about the origin for $A \ll |\mathbf{y}|$. The first-order terms are a stokeslet and a dipole. For convenience, define

$$W_{jk}(\mathbf{x}) = -\tfrac{3}{4}A\left(\frac{\delta_{jk}}{|\mathbf{x}|}+\frac{x_j x_k}{|\mathbf{x}|^3}\right)+\tfrac{1}{4}A^3\left(-\frac{\delta_{jk}}{|\mathbf{x}|^3}+\frac{3x_j x_k}{|\mathbf{x}|^5}\right). \tag{14}$$

The second-order terms include a Stokes-doublet and a potential quadrupole. It is convenient to divide these singularities into their symmetric and antisymmetric components and thus to define

$$W_{S_{jkl}}(\mathbf{x}) = -\tfrac{5}{2}A^3\left(\frac{-x_j\delta_{kl}}{|\mathbf{x}|^3}+\frac{3x_j x_k x_l}{|\mathbf{x}|^5}\right)+\tfrac{3}{2}A^5\left(-\frac{x_j\delta_{kl}+x_k\delta_{jl}+x_l\delta_{jk}}{|\mathbf{x}|^5}+\frac{5x_j x_k x_l}{|\mathbf{x}|^7}\right) \tag{15}$$

and

$$W_{A_{jkl}}(\mathbf{x}) = A^3\left(\frac{-\delta_{jk}x_l+\delta_{jl}x_k}{|\mathbf{x}|^3}\right). \tag{16}$$

With definitions (14), (15) and (16), the expansion for S^*_{jk} about the origin may be written as

$$S^*_{jk}(\mathbf{x},\mathbf{y}) = \left(\frac{\delta_{km}}{|\mathbf{y}|}+\frac{y_k y_m}{|\mathbf{y}|^3}\right)W_{jm}(\mathbf{x})+\left(\frac{y_k y_m y_n}{|\mathbf{y}|^5}\right)W_{S_{jmn}}(\mathbf{x})+\frac{y_m}{|\mathbf{y}|^3}W_{A_{jkm}}(\mathbf{x}), \tag{17}$$

where terms of order $O(A^2/|\mathbf{y}|^2)$ are neglected.

In terms of its $\mathbf{x}$ dependence, this expression does not appear much simpler than (9), but its dependence on $\mathbf{y}$ is of a form which is easily differentiated.

Recall that the Stokes-doublet was defined by $(\partial/\partial y_l)\, S_{jk}$. Applying the rule stated above for finding images of higher-order singularities, the image of the Stokes-doublet is given by $(\partial/\partial y_l) S^*_{jk}$. Differentiating (17) accordingly yields

$$S^*_{D_{jkl}}(\mathbf{x},\mathbf{y}) = -\left[\left(\frac{-y_m\delta_{kl}}{|\mathbf{y}|^3}+\frac{3y_k y_l y_m}{|\mathbf{y}|^5}\right)+\left(\frac{y_l\delta_{km}-y_k\delta_{lm}}{|\mathbf{y}|^3}\right)\right] W_{jm}(\mathbf{x})$$
$$-\left[-\frac{\delta_{kl}y_m y_n+\delta_{lm}y_k y_n+\delta_{ln}y_k y_m}{|\mathbf{y}|^5}+\frac{5y_k y_l y_m y_n}{|\mathbf{y}|^7}\right] W_{S_{jmn}}(\mathbf{x})$$
$$-\left[-\frac{\delta_{lm}}{|\mathbf{y}|^3}+\frac{3y_l y_m}{|\mathbf{y}|^5}\right] W_{A_{jkm}}(\mathbf{x}). \tag{18}$$

Note that the functions W_{jm}, $W_{S_{jmn}}$ and $W_{A_{jkm}}$ are exactly the same as in (17). This means that, to any order, the expansions for the image systems of the stokeslet and all its derivatives are composed of the same group of singularities. Only the strength of the singularities as expressed in the $\mathbf{y}$ dependence changes.

The image system for the dipole is found by calculating $-\frac{1}{2}\nabla^2_y S^*_{jk}$. Differentiating (17) yields

$$D^*_{jk}(\mathbf{x},\mathbf{y}) = \left[\frac{-\delta_{km}}{|\mathbf{y}|^3}+\frac{3y_k y_m}{|\mathbf{y}|^5}\right] W_{jm}(\mathbf{x})$$
$$+\left[-\frac{\delta_{km}y_n+\delta_{kn}y_m+\delta_{mn}y_k}{|\mathbf{y}|^5}+\frac{5y_k y_m y_n}{|\mathbf{y}|^7}\right] W_{S_{jmn}}(\mathbf{x}). \tag{19}$$

Note that, in this case, there is no W_A term, because $\nabla^2_y(y_m/|\mathbf{y}|^3) = 0$.

This completes the set of sphere images needed in this problem.

4. Image system for a plane

The solution of Stokes' equations in the half space is considerably simplified through the use of the Green's function for this domain. As with the Green's function described in § 3, this consists of a stokeslet plus a collection of images which cancel the velocity on the boundary. In this case, the boundary is a plane.

Let the origin of the co-ordinate system be a distance H from the plane boundary. Define the vector $\mathbf{p}$ as the unit vector perpendicular to the plane pointing *into* the fluid. A stokeslet at $\mathbf{y}$ is a distance $h(\mathbf{y})$ from the plane, where

$$h(\mathbf{y}) = H + \mathbf{y}.\mathbf{p}. \tag{20}$$

The image point $\breve{\mathbf{y}}$ of $\mathbf{y}$ is defined by

$$\breve{\mathbf{y}} = \mathbf{y} - 2h(\mathbf{y})\,\mathbf{p}. \tag{21}$$

The Green's function for the half space is

$$G_{P_{jk}}(\mathbf{x},\mathbf{y}) = S_{jk}(\mathbf{x},\mathbf{y}) + \breve{S}_{jk}(\mathbf{x},\mathbf{y}), \tag{22}$$

where $\breve{S}_{jk}$ is the image system for the plane.

The image system is defined by

$$\begin{aligned}\breve{S}_{jk}(\mathbf{x},\mathbf{y}) = & -S_{jk}(\mathbf{x},\breve{\mathbf{y}}) + 2h(\mathbf{y})\,p_l[\delta_{km}-2p_kp_m]\,S_{D_{jlm}}(\mathbf{x},\breve{\mathbf{y}}) \\ & -2h^2(y)\,[\delta_{km}-2p_kp_m]\,D_{jm}(\mathbf{x},\breve{\mathbf{y}}).\end{aligned} \tag{23}$$

This image system consists of a stokeslet, Stokes-doublet and dipole at the image point $\breve{\mathbf{y}}$. This is much simpler than the image system for a sphere, as it contains no distributed singularities.

The expression for the image system in (23) was given in a slightly different form by Blake (1971). Alternatively, it can be obtained from (9) as the limit for a sphere of infinite radius.

5. Combined image system

In this section, the results of §§ 3 and 4 are combined to obtain an approximate expression for the Green's function for the flow external to a sphere in the half space. The combined image system is more complicated than the sum of the two individual image systems, because it contains terms due to the interaction of the two image systems.

Let the origin of the co-ordinate system be at the centre of the sphere. The sphere has radius A, and its centre is a distance H from the plane. As before, the vector $\mathbf{p}$ is defined as the unit vector perpendicular to the plane pointing into the fluid (see figure 1).

To construct the combined image system, we start with the image systems for the plane and the sphere. Each of these image systems cancels the velocity of the stokeslet on its respective boundary, but induces a non-zero velocity on the other boundary. To cancel this velocity, we add the plane image of the sphere image and the sphere image of the plane image. These images, in their turn, cancel the velocity on one boundary, but induce a non-zero velocity on the other. Thus, the process must be repeated with the images of the next order.

There is one difference between the plane images and the sphere images which make it possible to obtain an approximate expression for the combined image system after a finite number of terms. The plane images are a large distance $O(H)$ from both the plane and the sphere and induce a velocity of the same order on both boundaries. The sphere images are a distance A from the surface of the sphere, but are a distance H from the plane. Thus, an nth-order image singularity in the sphere induces a velocity at the plane order $O(A^n/H^n)$ with respect to the velocity it induces on the sphere. When the sphere images are added to cancel a certain velocity on the sphere, they induce a lower-order velocity on the plane; hence, the velocity on both surfaces is reduced by a factor A/H at the end of each cycle of plane–sphere reflexions. A second result is that, to order $O(A^2/H^2)$, the calculation of plane images of sphere images need consider only the stokeslets in the sphere.

The first approximation to the Green's function is the sum of the Stokeslet plus the two individual image systems,

$$G_{jk}(\mathbf{x},\mathbf{y}) \approx S_{jk}(\mathbf{x},\mathbf{y}) + S^*_{jk}(\mathbf{x},\mathbf{y}) + \breve{S}_{jk}(\mathbf{x},\mathbf{y}), \tag{24}$$

where the terms are defined by (1), (9) and (23) respectively.

Consider the problem of finding the sphere images of the plane image system $\breve{S}_{jk}$.

This image system consists of a stokeslet, Stokes-doublet and dipole. Its image in the sphere is obtained by replacing each of these singularities with its respective image in the sphere. The necessary expressions were derived in § 3.

The sphere images of the plane images are expressed as

$$\begin{aligned}\overset{*}{\breve{S}}_{jk}(\mathbf{x},\mathbf{y}) = &-S^*_{jk}(\mathbf{x},\breve{\mathbf{y}}) + 2h(\breve{\mathbf{y}})\,p_l[\delta_{km}-p_kp_m]\,S^*_{Djlm}(\mathbf{x},\breve{\mathbf{y}}) \\ &-2h^2(\mathbf{y})\,[\delta_{km}-p_kp_m]\,D^*_{jm}(\mathbf{x},\breve{\mathbf{y}}),\end{aligned} \tag{25}$$

where S^*_{jk}, S^*_{Djlm} and D^*_{jm} are given by (17), (18) and (19) respectively. Note that, in this case, the approximate form of S^*_{jk} may be used, because the stokeslet is a large distance from the sphere.

Adding (25) to (24), the approximate expression for the Green's function now has the form

$$G_{jk}(\mathbf{x},\mathbf{y}) \approx S_{jk}(\mathbf{x},\mathbf{y}) + S^*_{jk}(\mathbf{x},\mathbf{y}) + \breve{S}_{jk}(\mathbf{x},\mathbf{y}) + \overset{*}{\breve{S}}_{jk}(\mathbf{x},\mathbf{y}). \tag{26}$$

This expression satisfies the boundary condition on the sphere to $O(A^2/H^2)$, but the velocity at the plane boundary is $O(A/H)$. This velocity is due to terms in S^*_{jk} and $\breve{S}_{jk}$ whose plane images have not been considered. The leading terms of these functions are stokeslets at the origin of the form

$$-\tfrac{3}{4}AS_{kl}(0,\mathbf{y})\,S_{jl}(\mathbf{x},0) - \tfrac{3}{4}A\breve{S}_{kl}(0,\mathbf{y})\,S_{jl}(\mathbf{x},0). \tag{27}$$

Since these terms are merely stokeslets, their images in the plane are obtained by replacing $S_{jl}(\mathbf{x},0)$ with $\breve{S}_{jl}(\mathbf{x},0)$. Thus, the plane images of (27) are expressed as

$$-\tfrac{3}{4}AS_{kl}(0,\mathbf{y})\,\breve{S}_{jl}(\mathbf{x},0) - \tfrac{3}{4}A\breve{S}_{kl}(0,\mathbf{y})\,\breve{S}_{jl}(\mathbf{x},0). \tag{28}$$

The addition of this term to (26) corrects the velocity on the plane, but induces a velocity on the sphere $O(A/H)$. To cancel this velocity, the sphere image of (28) must be added. This is obtained by replacing $\breve{S}_{jl}(\mathbf{x},0)$ with $\overset{*}{\breve{S}}_{jl}(\mathbf{x},0)$ to yield

$$-\tfrac{3}{4}AS_{kl}(0,\mathbf{y})\,\overset{*}{\breve{S}}_{jl}(\mathbf{x},0) - \tfrac{3}{4}A\breve{S}_{kl}(0,\mathbf{y})\,\overset{*}{\breve{S}}_{jl}(\mathbf{x},0). \tag{29}$$

Adding (28) and (29) to the Green's function (26) gives the following expression for the combined Green's function,

$$\begin{aligned}G_{jk}(\mathbf{x},\mathbf{y}) = &\,S_{jk}(\mathbf{x},\mathbf{y}) + S^*_{jk}(\mathbf{x},\mathbf{y}) + \breve{S}_{jk}(\mathbf{x},\mathbf{y}) + \overset{*}{\breve{S}}_{jk}(\mathbf{x},\mathbf{y}) \\ &-\tfrac{3}{4}A[S_{kl}(0,\mathbf{y}) + \breve{S}_{kl}(0,\mathbf{y})]\,[\breve{S}_{jl}(\mathbf{x},0) + \overset{*}{\breve{S}}_{jl}(\mathbf{x},0)].\end{aligned} \tag{30}$$

This expression is a solution of Stokes' equations which includes the fundamental solution and satisfies the boundary conditions on the sphere and plane to $O(A^2/H^2)$. Therefore, it is the correct expression for the combined Green's function to $O(A^2/H^2)$.

The velocity at $\mathbf{x}$ due to a stokeslet of strength $\mathbf{f}$ at $\mathbf{y}$ in the presence of a sphere in the half space is

$$u_j(\mathbf{x}) = G_{jk}(\mathbf{x},\mathbf{y})f_k/8\pi\mu. \tag{31}$$

6. Velocity induced by singularity distributions

The application of slender body theory to problems involving flagellar motions was described in I. The principal result is that the flagellum may be represented by distributions of stokeslets and dipoles along its centre-line. To satisfy the boundary condition on other surfaces, the stokeslet is replaced by the Green's function applicable

to the geometry of the problem. For the current problem, the stokeslet is replaced by the Green's function (30) derived in § 5.

Let the origin of the co-ordinate system be at the centre of the sphere. The relative positions of the sphere and plane are as previously specified. The shape of the flagellum is specified by a function $\mathbf{X}(s)$, where s is the arclength measured from the point at which the flagellum meets the sphere.

The velocity induced by the singularity distributions along the flagellum and their images is given by

$$u_j(\mathbf{x}) = \int_0^L \left[G_{jk}(\mathbf{x}, \mathbf{X}(s)) \frac{f_k(s)}{8\pi\mu} + D_{jk}(\mathbf{x}, \mathbf{X}(s)) \frac{d_k(s)}{4\pi} \right] ds, \tag{32}$$

where **f** and **d** are the stokeslet and dipole strengths and the integration extends along the flagellum. The functions G_{jk} and D_{jk} are defined by (30) and (5) respectively.

It was shown in I that the dipole strength is determined by the component of the stokeslet normal to the centre-line. In particular

$$d_k = \frac{-a^2}{4\mu} (\delta_{kl} - T_k T_l) f_l, \tag{33}$$

where **T** is the unit vector tangent to the flagellum, and a is the radius of the flagellum.

It is convenient to divide the Green's function G_{jk} into two terms: the stokeslet S_{jk} and the image system $S^{\ominus}_{jk}$.

The function $S^{\ominus}_{jk}$ represents the sum of all the image terms derived in § 5 and may be defined as

$$S^{\ominus}_{jk}(\mathbf{x}, \mathbf{y}) = G_{jk}(\mathbf{x}, \mathbf{y}) - S_{jk}(\mathbf{x}, \mathbf{y}), \tag{34}$$

where G_{jk} and S_{jk} are given by (30) and (1).

The induced velocity may now be written in the form

$$u_j(\mathbf{x}) = \int_0^L \left\{ [S_{jk}(\mathbf{x}, \mathbf{X}(s)) + S^{\ominus}_{jk}(\mathbf{x}, \mathbf{X}(s))] \frac{f_k(s)}{8\pi\mu} + D_{jk}(\mathbf{x}, \mathbf{X}(s)) \frac{d_k(s)}{4\pi} \right\} ds. \tag{35}$$

This integral is evaluated by dividing the flagellum into N intevals in which **f** is assumed constant. The image system $S^{\ominus}_{jk}$ is singular inside the sphere and at the image points in the plane, but it is well behaved along the flagellum. Thus, it may be integrated easily by numerical methods.

Let the nth interval have midpoint s_n and length $2\delta s_n$. The integral of $S^{\ominus}_{jk}$ in this interval is designated:

$$H_{jk}(\mathbf{x}, \mathbf{X}(s_n)) = \frac{1}{8\pi\mu} \int_{s_n - \delta s_n}^{s_n + \delta s_n} S^{\ominus}_{jk}(\mathbf{x}, \mathbf{X}(s))\, ds \tag{36}$$

with the understanding that the integral is evaluated numerically.

The functions S_{jk} and D_{jk} in (35) may be integrated analytically. Using (33) to eliminate **d** and employing the results of the integrations, the induced velocity may be written in the form

$$u_j(\mathbf{x}) = \sum_{n=1}^{N} \{ [K_{jk}(\mathbf{x}, \mathbf{X}(s_n)) + H_{jk}(\mathbf{x}, \mathbf{X}(s_n))] f_k(s_n) \}, \tag{37}$$

where $f_k(s_n)$ is the value of **f** in the nth interval, and K_{jk} represents the terms integrated analytically. The exact expression for K_{jk} is given in I, equation (27).

The expression (37) gives the velocity induced by the singularity distributions along the flagellum and their images in the plane and the sphere.

7. Kinematics of flagellar motion

In this section, we consider the specification of the shape of the flagellum and the determination of the velocity of points on the flagellum. We assume that the shape of the flagellum as a function of time is given in the form

$$(X, Y, Z) = (X, Y(X,t), 0). \tag{38}$$

Let the point of contact of the flagellum with the cell body be $\mathbf{X}_0$. The arclength s measured from the base of the flagellum at $\mathbf{X}_0$ is given by

$$s = \int_{X_0}^{X} \left[1 + \left(\frac{\partial Y}{\partial X}\right)^2\right]^{\frac{1}{2}} dX. \tag{39}$$

It has been assumed that the flagellum is inextensible. Thus, the velocity of a point on the flagellum is given by

$$\mathbf{u} = \frac{\partial}{\partial t}\mathbf{X}(s,t). \tag{40}$$

When the shape of the flagellum is expressed in the form (38), this expression cannot be evaluated directly. Instead, the chain rule for partial differentiation is used to obtain the velocity in the form

$$\mathbf{u} = \left(\frac{\partial X(s,t)}{\partial t}, \frac{\partial Y(X,t)}{\partial t} + \frac{\partial Y(X,t)}{\partial X}\frac{\partial X(s,t)}{\partial t}, 0\right). \tag{41}$$

The derivative $\partial X/\partial t$ may be evaluated by applying the rule for differentiating implicit functions to (39) to yield

$$\frac{\partial X}{\partial t}(s,t) = -\left[1 + \left(\frac{\partial Y}{\partial X}\right)^2\right]^{-\frac{1}{2}} \int_{X_0}^{X} \left(\frac{\partial Y}{\partial X}\right)\left(\frac{\partial^2 Y}{\partial X\,\partial t}\right)\left[1 + \left(\frac{\partial Y}{\partial X}\right)^2\right]^{-\frac{1}{2}} dX. \tag{42}$$

The velocity of points on the flagellum is given by (41) and (42) when the shape of the flagellum is given in the form (38).

At this point, it is necessary to specify the wave form to be used in the present problem. As mentioned previously, the observed wave forms are approximately sinusoidal. Consider first a wave of the form

$$Y(X,t) = \alpha \sin\left[k(X - X_0) + \phi(t)\right]. \tag{43}$$

This wave has constant amplitude and wavenumber, with unspecified time dependence. If a wave of this form is employed, the condition that the flagellum is attached to the cell body radially cannot be satisfied. To overcome this difficulty, the amplitude of the wave is modified by the function

$$E(x) = 1 - \exp\left[-(k_E x)^2\right]. \tag{44}$$

This function has the properties that $E(0) = 0$, $E'(0) = 0$ and $E(x)$ grows very rapidly to its asymptotic value $E(\infty) = 1$.

Multiplying (43) by $E(X - X_0)$ yields a sinusoidal wave of the form

$$Y(X,t) = E(X - X_0)\,\alpha \sin\left[k(X - X_0) + \phi(t)\right]. \tag{45}$$

This wave has a small 'end region' in which its amplitude grows very quickly, after which it forms a constant amplitude, constant wavenumber sine wave.

The functional form of $\phi(t)$ which most closely approximates the actual waves used by organisms is a matter of some uncertainty. It is relatively easy to obtain the function $Y(X)$ from photographs of the organism, but it is more difficult to obtain accurate information regarding the form of $\phi(t)$.

In the present work, we assume that $\phi(t)$ is of a form such that the fully developed wave has constant curvilinear wave speed c. This type of wave has often been used in studying locomotion and is consistent with the waves employed in I.

For the fully developed wave to have constant curvilinear wave speed c, we require that $Y(s,t)$ be of the form $Y(s-ct)$ when s (or X) is large. This condition is expressed:

$$\lim_{s\to\infty}\left\{\frac{\partial}{\partial t}Y(s,t) = -c\frac{\partial}{\partial s}Y(s,t)\right\}. \tag{46}$$

To find $\phi(t)$, we convert these derivatives to functions of s, X and ϕ.

Applying the chain rule to the left-hand side yields

$$\frac{\partial}{\partial t}Y(s,t) = \frac{\partial Y(X,\phi)}{\partial X}\frac{\partial X(s,t)}{\partial t} + \frac{\partial Y(X,\phi)}{\partial \phi}\frac{d\phi}{dt}, \tag{47}$$

and further

$$\frac{\partial}{\partial t}Y(s,t) = \left[\frac{\partial Y(X,\phi)}{\partial X}\frac{\partial X(s,\phi)}{\partial \phi} + \frac{\partial Y(X,\phi)}{\partial \phi}\right]\frac{d\phi}{dt}. \tag{48}$$

From (45) we note that

$$\lim_{X\to\infty}\left\{\frac{\partial}{\partial X}Y(X,\phi) = k\frac{\partial}{\partial \phi}Y(X,\phi)\right\} \tag{49}$$

and hence from (48),

$$\lim_{s\to\infty}\left\{\frac{\partial}{\partial t}Y(s,t) = \left[1+k\frac{\partial X(s,\phi)}{\partial \phi}\right]\frac{\partial Y(X,\phi)}{\partial \phi}\frac{d\phi}{dt}\right\}. \tag{50}$$

Applying the chain rule to the right-hand side of (46) yields

$$-c\frac{\partial}{\partial s}Y(s,t) = -c\frac{\partial Y(X,\phi)}{\partial X}\frac{\partial X(s,\phi)}{\partial s}. \tag{51}$$

Taking the limit and employing (49) yields

$$\lim_{s\to\infty}\left\{-c\frac{\partial}{\partial s}Y(s,t) = -kc\frac{\partial Y(X,\phi)}{\partial \phi}\frac{\partial X(s,\phi)}{\partial s}\right\}. \tag{52}$$

Equating (50) and (52) gives an expression for $d\phi/dt$,

$$\frac{d\phi}{dt} = \lim_{s\to\infty}\left\{\frac{-kc\dfrac{\partial X(s,\phi)}{\partial s}}{1+k\dfrac{\partial X(s,\phi)}{\partial \phi}}\right\}. \tag{53}$$

Equation (53) gives $d\phi/dt$ as a function of ϕ. Choosing initial condition $\phi = 0$ at $t = 0$ and integrating gives ϕ in the implicit form

$$t = \int_0^{\phi}\left[\frac{d\phi}{dt}\right]^{-1}d\phi. \tag{54}$$

The period of the wave τ is defined by

$$\tau = \int_0^{2\pi} \left[\frac{d\phi}{dt}\right]^{-1} d\phi. \tag{55}$$

After making substitutions from (45) and (53), this can be written in the form

$$\tau = \frac{1}{kc}\int_0^{2\pi} [1+\alpha^2 k^2 \cos^2\phi]^{\frac{1}{2}}\, d\phi. \tag{56}$$

This expression is merely a statement of the fact that the period equals the curvilinear wavelength divided by the curvilinear wave speed. The linear wavelength λ equals $2\pi/k$, and the linear wave speed V equals λ/τ.

This completes the specification of the flagellar motion.

8. Solution of equations

The boundary condition on the flagellum requires that the induced velocity (37) equal the velocity of the flagellum (41). The induced velocity (37) depends on the $2N$ values of $\mathbf{f}(s_n)$. To obtain a system of $2N$ equations, the boundary condition is imposed at the centre of each segment of the flagellum. The resulting equations are of the form

$$u_j(\mathbf{X}(s_m)) = \sum_{n=1}^{N} \{[K_{jk}(\mathbf{X}(s_m), \mathbf{X}(s_n)) + H_{jk}(\mathbf{X}(s_m), \mathbf{X}(s_n))] f_k(s_n)\}, \tag{57}$$

where $\mathbf{u}(\mathbf{X}(s_m))$ is the velocity of the flagellum at the midpoint of the mth segment, and the summation gives the induced velocity at that point.

At an instant of time, (57) represents a system of $2N$ linear algebraic equations in the $2N$ unknowns, $\mathbf{f}(s_n)$. This system of equations is solved by an iteration process. To rewrite (57) in a more convenient form, we make the following definitions:

$$Q_{jk}(s_m, s_n) = K_{jk}(\mathbf{X}(s_m), \mathbf{X}(s_n)) + H_{jk}(\mathbf{X}(s_m), \mathbf{X}(s_n)) \tag{58}$$

and

$$P_{jk}(s_m) = \sum_{n=1}^{N} Q_{jk}(s_m, s_n). \tag{59}$$

The boundary condition (57) may now be written in the form

$$u_j(s_m) = P_{jk}(s_m) f_k(s_m) + \sum_{n=1}^{N} [f_k(s_n) - f_k(s_m)]\, Q_{jk}(s_m, s_n). \tag{60}$$

Multiplying (60) by the inverse of P_{jk} and rearranging yields

$$f_l(s_m) = [P(s_m)]^{-1}_{lj} \left\{ u_j(s_m) - \sum_{n=1}^{N} [f_k(s_n) - f_k(s_m)]\, Q_{jk}(s_m, s_n) \right\}. \tag{61}$$

This expression is used to define the iteration process. The right-hand side of the equation depends on the previous values of $\mathbf{f}$, while the left-hand side defines the next iteration. This process converges to yield a solution for $\mathbf{f}$ at an instant of time.

The purpose of the flagellar motion is to produce a flow which is filtered by the collar of the organism to extract food particles. To determine the optimal flagellar motion, we require a measure of the effectiveness of this process. The average flow through the collar is the most logical measure of the flow rate, but this quantity is difficult to

evaluate. Instead, we choose a simpler measure – the average flow through a disk tangent to the surface of the sphere at the point of contact of the flagellum. For a disk of the proper radius, this quantity is identical to the flow through the collar. The radius of the disk is chosen to be twice the radius of the cell body, a size which corresponds roughly to the effective area of the collar.

The average flow rate through the disk is

$$U = \frac{1}{4\pi A^2}\int_0^{2A}\int_0^{2\pi} \mathbf{u}(\mathbf{r}) \cdot \mathbf{p}\, r\, dr\, d\theta, \tag{62}$$

where $\mathbf{p}$ is the unit vector perpendicular to the disk (and to the plane), $\mathbf{u}$ is the induced velocity, and the integration extends over the area of the disk. The flow rate U is analogous to the swimming speed of an organism employing its flagellum for locomotion. A disk moving through the fluid at speed U would be equivalent to a flow rate U. In addition to the flow rate, we need to know the power consumption of the organism. The instantaneous power is given by

$$P = \sum_{n=1}^{N} [\mathbf{f}(s_n) \cdot \mathbf{u}(s_n)]\, 2\delta s_n, \tag{63}$$

where $\mathbf{u}$ is the velocity of the flagellum, $\mathbf{f}$ is the force distribution and $2\delta s_n$ is the length of the nth segment of the flagellum.

The flow rate and power consumption defined by (62) and (63) respectively are the instantaneous values of these quantities. To obtain the time average of the quantities, the equations must be solved at several points in the cycle of the wave, and the results used to evaluate the expressions

$$\overline{U} = \frac{1}{\tau}\int_0^{\tau} U(t)\, dt \quad \text{and} \quad \overline{P} = \frac{1}{\tau}\int_0^{\tau} P(t)\, dt. \tag{64}$$

The number of points required in the various summations and details of the computing are given in the appendix.

9. Results

In this section, we examine the dependence of the flow rate and power consumption on the parameters. The dimensions of the organism determine the three body parameters: a/A, L/A and H/A, where a is the flagellar radius, L is the flagellar length, A is the cell body radius and H is the height of the cell body above the plane substrate. The shape of the wave is specified by the three wave parameters: N_λ, αk and k/k_E. N_λ is the number of linear wavelengths on the wave; the other parameters are as they appear in (44) and (45).

The average flow rate is non-dimensionalized in the form $\overline{U}/V$, where V is the average linear wave speed. The power consumption is non-dimensionalized as

$$\eta^{-1} = \overline{P}/6\pi\mu A\, \overline{U}^2. \tag{65}$$

This expression gives the power required to produce a given flow rate. Its minimum occurs at the optimal combination of the parameters, hence it is called the inverse efficiency.

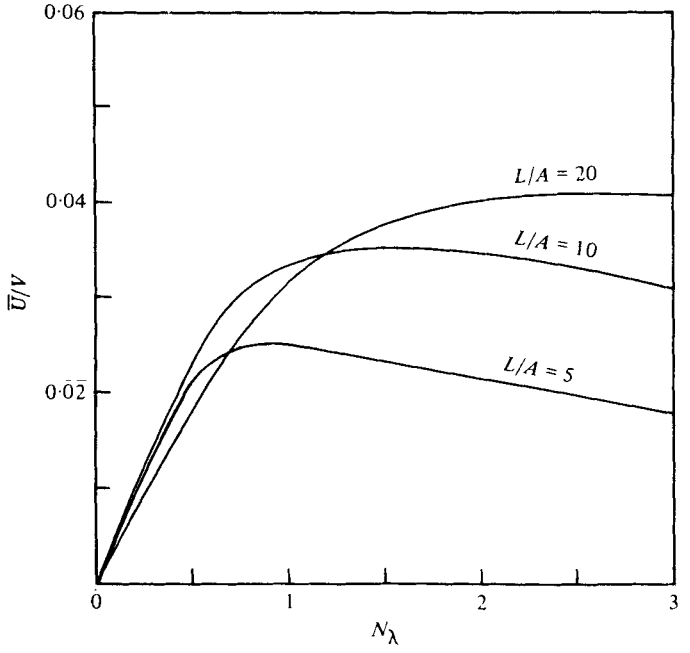

FIGURE 2. Average flow rate as a function of number of waves, N_λ, for three different length flagella, radius $a/A = 0{\cdot}02$. (Height $H/A = 10$. Wave parameters: $\alpha k = 2$, $k/k_E = 1$.)

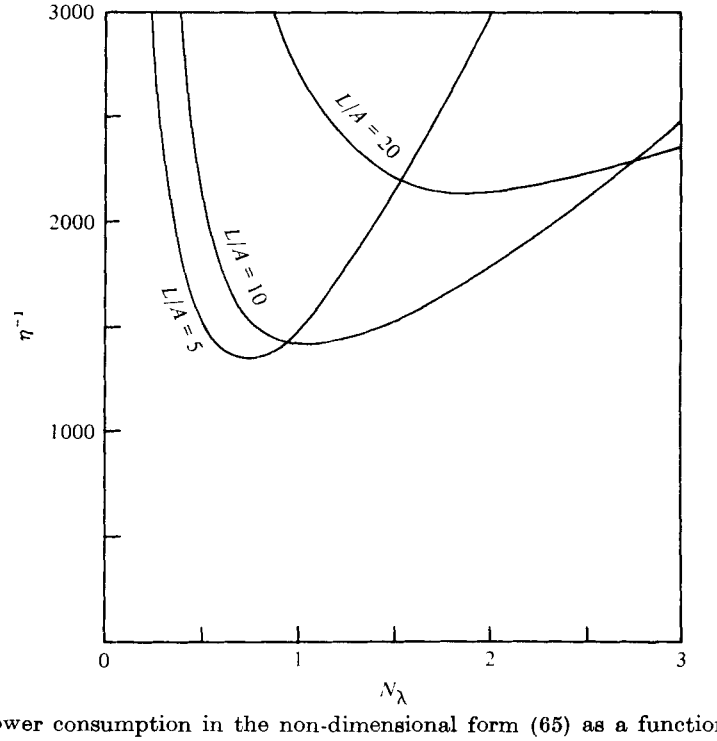

FIGURE 3. Power consumption in the non-dimensional form (65) as a function of number of waves, N_λ, for three different length flagella, radius $a/A = 0{\cdot}02$. (Height $H/A = 10$. Wave parameters: $\alpha k = 2$, $k/k_E = 1$.)

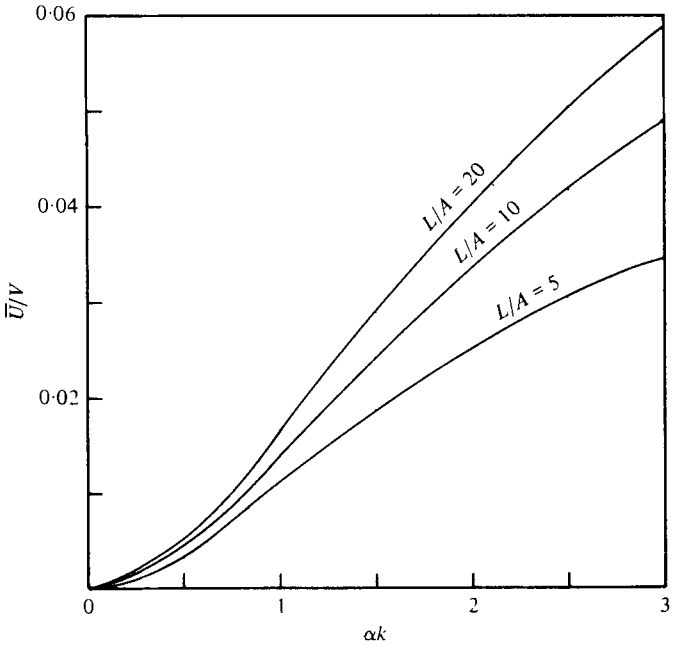

FIGURE 4. Average flow rate as a function of αk for three different length flagella with radius $a/A = 0{\cdot}02$. (Height $H/A = 10$. Wave parameters: optimum N_λ, $k/k_E = 1$.)

In the following discussion, variation of the wave parameters is considered first, followed by variation of the body parameters.

The average flow rate as a function of N_λ is shown in figure 2. The curves are plotted for three different length flagella with fixed values for the other parameters. For motions in which the entire flagellum forms only a fraction of a wavelength ($N_\lambda < 1$), the flow produced is very irregular, and the net flow over the cycle is small. As the number of wavelengths increases, the flow becomes more uniform, and the average flow rate increases. The maximum flow rate $\overline{U}/V$ is produced at $N_\lambda = 1$ for $L/A = 10$. For longer flagella, the value of N_λ for maximum flow rate increases linearly with the flagellar length. For shorter flagella, the maximum flow occurs at a value of N_λ marginally less than 1. The slow decline in flow rate for N_λ greater than its optimum value is due to interference with the cell body. The velocity induced by the flagellar motion is concentrated within the envelope of the wave. As the number of wavelengths is increased, the amplitude of the wave decreases, and the flow is confined to a column of smaller diameter. The axis of this column passes through the centre of the sphere. Thus, as the flow becomes more concentrated along the axis, the interference with the cell body becomes greater. The optimum N_λ increases linearly with flagellar length, because this rate of increase holds the diameter of the column constant.

The non-dimensional power η^{-1} as a function of N_λ is shown in figure 3. The actual power $\overline{P}$ increases slowly with N_λ, because increasing the number of wavelengths decreases the ratio λ/a. As shown in the analysis of locomotion in I, the effectiveness of the flagellar motion depends on this ratio being large. Despite the gradual increase in power, the behaviour of η^{-1} in figure 3 is dominated by its dependence on the flow rate $\overline{U}$. Thus, the optimum value of N_λ is very close to the value which yields the

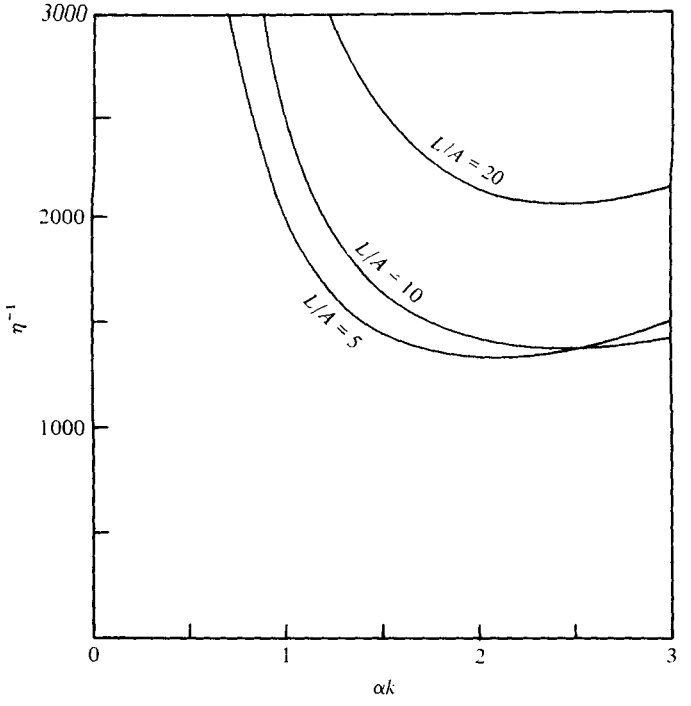

FIGURE 5. Power consumption (65) as a function of αk for three different length flagella with radius $a/A = 0{\cdot}02$. (Height $H/A = 10$. Wave parameters: optimum N_λ, $k/k_E = 1$.)

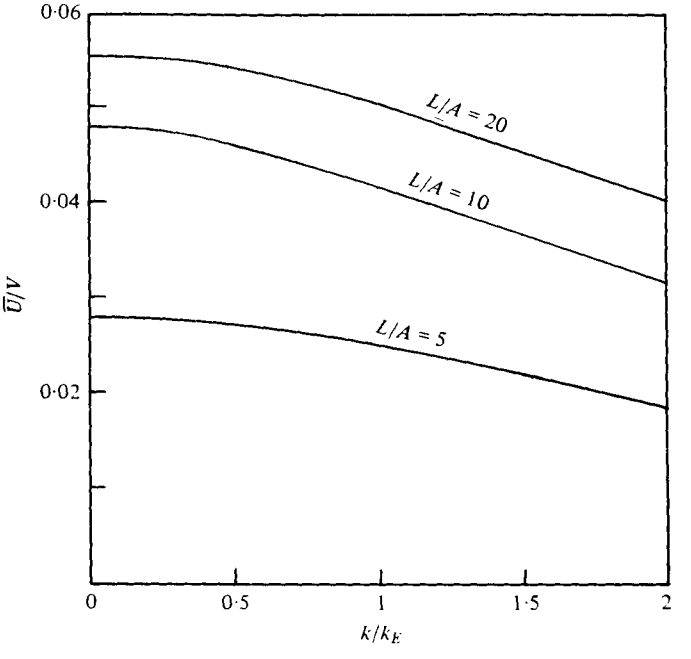

FIGURE 6. Average flow rate as a function of k/k_E for three different length flagella with radius $a/A = 0{\cdot}02$. (Height $H/A = 10$. Wave parameters: optimum N_λ and αk.)

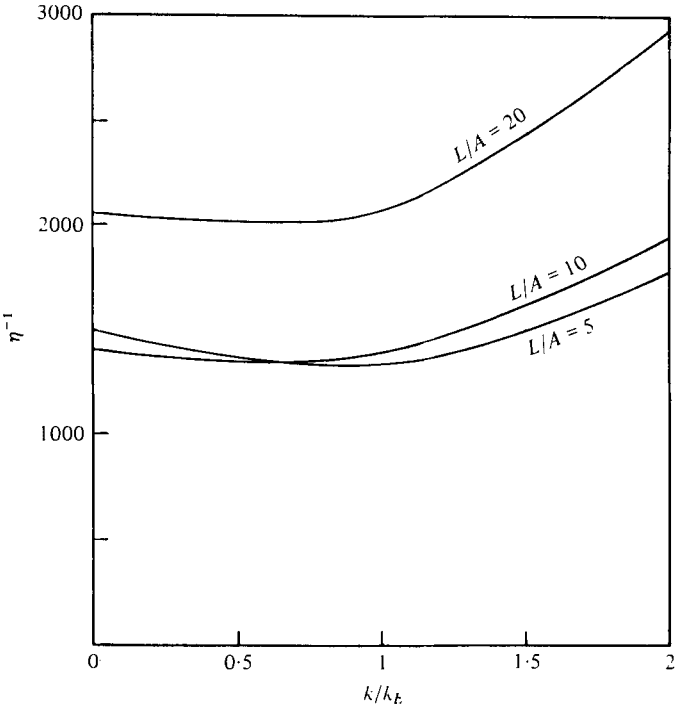

FIGURE 7. Power consumption (65) as a function of k/k_E for three different length flagella with radius $a/A = 0{\cdot}02$. (Height $H/A = 10$. Wave parameters: optimum N_λ and αk.)

maximum flow rate. The optimum value is $N_\lambda = 1$ for $L/A = 10$. For $L/A > 10$, the optimum value of N_λ increases linearly with L/A. For $L/A < 10$, the optimum number of wavelengths is marginally less than 1.

The flow rate as a function of αk is shown in figure 4. This parameter equals the maximum slope of the wave: the higher αk, the steeper the wave. In each case, the velocity increases nearly linearly with αk. This is in contrast to the behaviour for locomotion, for which the swimming speed levels off at a value of $\alpha k \approx 2$. The difference is due to the fact that the sessile organism is anchored to the substrate. In the case of locomotion, the increased thrust at higher αk is cancelled by the increased drag on the flagellum. In this case, the drag on the flagellum does not affect the flow rate directly, but only through its effect on the force distribution. Thus, the flow rate does not level off until the wave is much steeper.

The power consumption η^{-1} as a function of αk is shown in figure 5. The optimum value of αk is approximately 2·5 ($\alpha k = 2$ for the shortest flagellum, $L/A = 5$). The decrease in η^{-1} leading up to the optimum αk is due to the increase in flow rate as αk increases. The slow increase in η^{-1} for αk larger than the optimum is due to interference between neighbouring waves. There is a fundamental difference between this type of interference and that which occurs in locomotion. In locomotion, the primary cause of interference is the resistance encountered by a segment of the flagellum as it moves through the flow generated in the flow direction by other segments of the flagellum. In the sessile case, the points on the flagellum have negligible velocity in the wave direction. They move across the induced flow and do not experience an

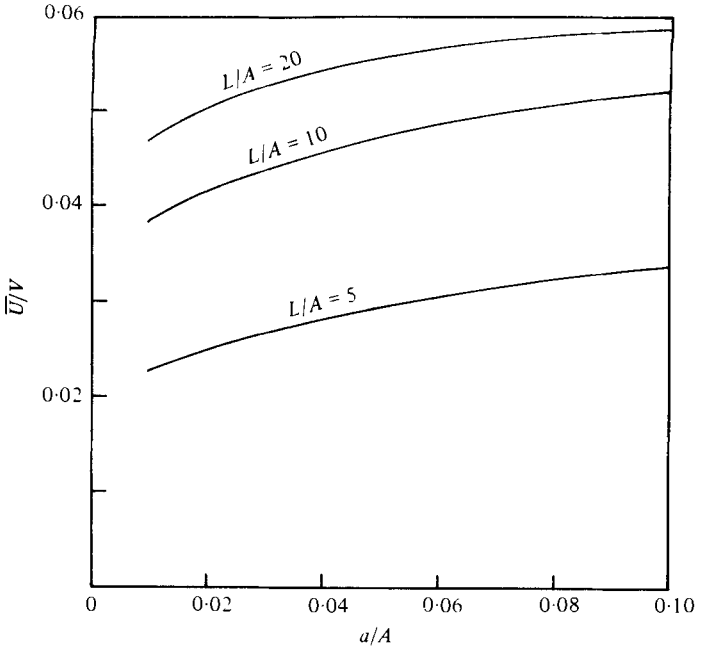

FIGURE 8. Average flow rate as a function of flagellar radius for three different length flagella. (Height $H/A = 10$. Optimum values for wave parameters.)

increase in power consumption as a result of increased flow in the wave direction. As the wave becomes very steep ($\alpha k > 3$), the interference due to transverse flow becomes significant, because alternate segments of the flagellum travel in opposite directions across the flow. This type of interference does not occur until the wave is much steeper; hence, the optimum slope for the sessile organisms is much higher than for locomotion.

The flow rate as a function of k/k_E is shown in figure 6. The parameter k/k_E is a measure of the distance required for the wave to reach its maximum amplitude. The flow rate has its maximum at $k/k_E = 0$, and decreases monotonically as k/k_E increases. This occurs because the amplitude of the wave in the vicinity of the cell body decreases exponentially with k/k_E. The decrease in velocity is gradual over the range of k/k_E considered, but the velocity decreases much more rapidly for higher values of k/k_E. For these values, the amplitude of the wave is diminished over a large part of the flagellum. This does not correspond to observed wave forms, and the flow rate for these values is not shown.

The power consumption η^{-1} as a function of k/k_E is shown in figure 7. The behaviour is consistent with figure 6. That is, η^{-1} increases as k/k_E increases due to the decreasing flow rate. Once again, the change is gradual over the range considered. Thus, we conclude that the optimum motion is relatively insensitive to the exact form of the wave at its junction with the cell body.

At this point, it is worthwhile summarizing the results for the wave parameters. The optimum number of waves on the flagellum is found to be directly proportional to the length of the flagellum when $L/A \geqslant 10$, with an optimum value $N_\lambda = 1$ at this length. For shorter flagella, the optimum N_λ is approximately 1. For the longer

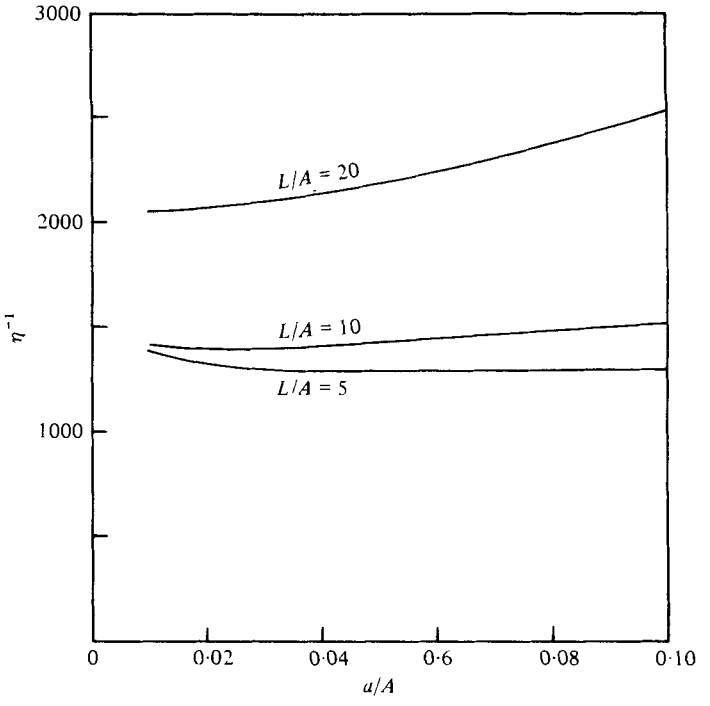

FIGURE 9. Power consumption (65) as a function of flagellar radius for three different length flagella. (Height $H/A = 10$. Optimum values for wave parameters.)

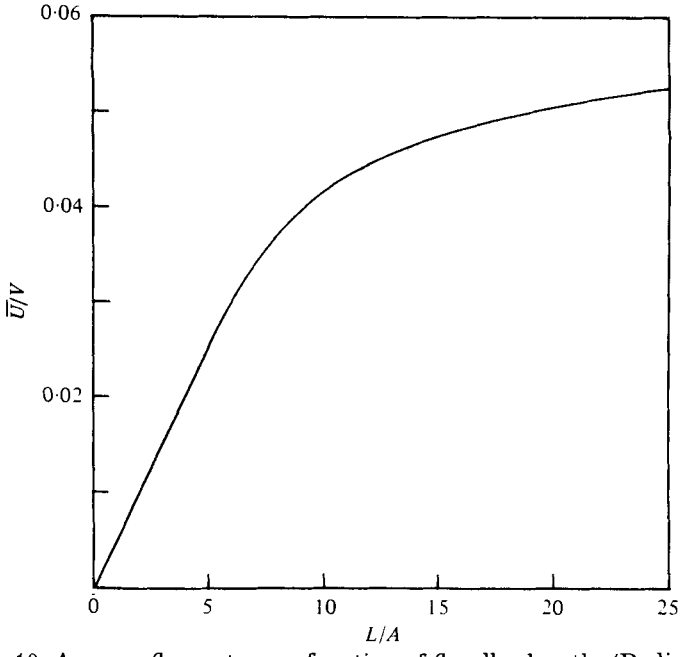

FIGURE 10. Average flow rate as a function of flagellar length. (Radius $a/A = 0{\cdot}02$, height $H/A = 10$. Optimum values for wave parameters.)

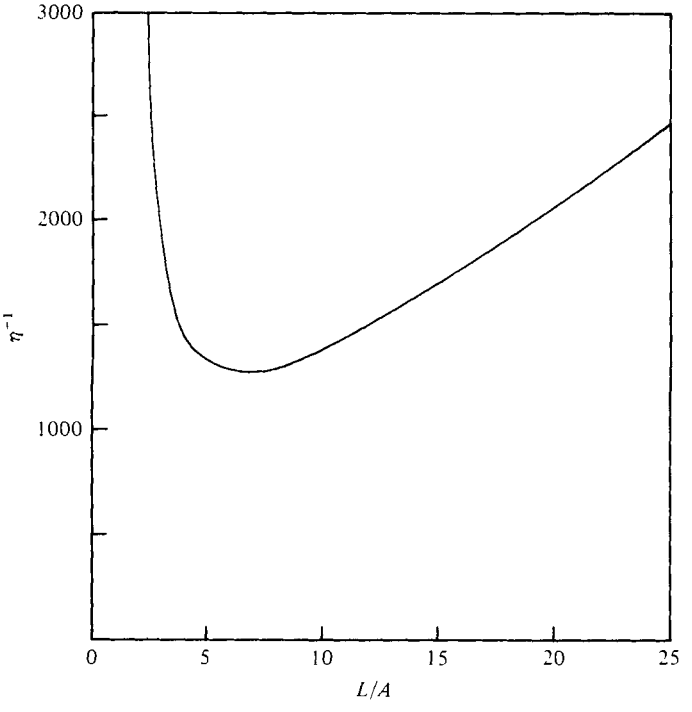

FIGURE 11. Power consumption (65) as a function of flagellar length. (Flagellar radius $a/A = 0{\cdot}02$, height $H/A = 10$. Optimum values for wave parameters.)

flagellum, this yields a constant ratio of curvilinear wavelength Λ to cell body radius A irrespective of the length of the flagellum. The optimum value of αk is in the range $2 < \alpha k < 2{\cdot}5$, which means that the slope of the wave is much steeper than the slope for optimal swimming. The combination of the optima for N_λ and αk yields the result that the optimum amplitude is approximately equal to the radius of the disk through which the flow is measured. Finally, the efficiency of the motion is relatively insensitive to the value of k/k_E.

Consider now the dependence of the flow rate and power consumption on the body parameters. Figure 8 shows the flow rate as a function of flagellar radius. The velocity increases monotonically as the radius increases. This is to be expected, because the thicker flagellum has a greater effect on the flow. The increase is gradual, because the dependence on a is logarithmic.

The dependence of η^{-1} on flagellar radius a/A is shown in figure 9. The non-dimensional power consumption η^{-1} shows negligible variation, because the increased power required to move the thicker flagellum is offset by the increased flow. Thus, there is no optimum flagellar radius.

The flow rate as a function of flagellar length is shown in figure 10. The velocity increases monotonically with increasing flagellar length. The increase in $\bar{U}/V$ is very rapid up to $L/A = 10$, after which it levels off and shows little increase. The addition of extra flagellar length past $L/A = 10$ has little effect, because the extra length is far from the cell body, and thus has less influence than segments of the flagellum closer to the cell body.

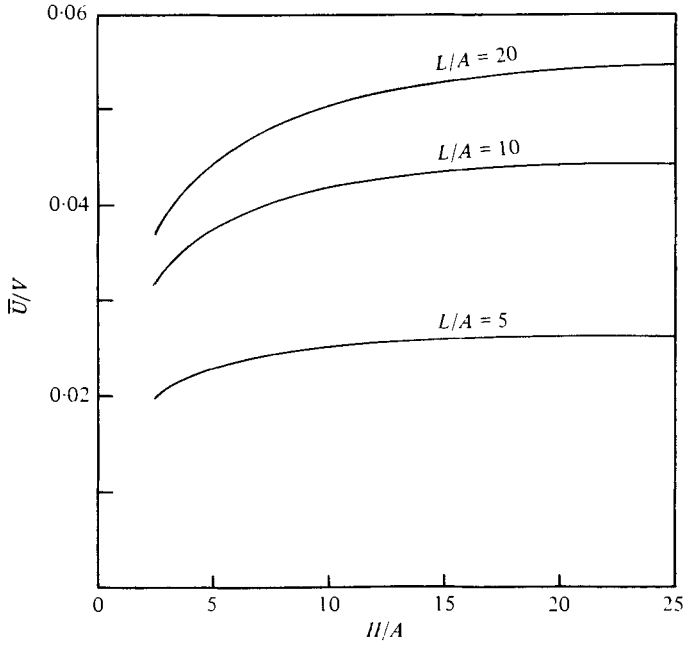

FIGURE 12. Average flow rate as a function of height for three different length flagella with radius $a/A = 0{\cdot}02$. (Optimum values for wave parameters.)

The power consumption as a function of flagellar length is shown in figure 11. There is a pronounced minimum at $L/A = 7$. For flagella shorter than this, the entire length of the flagellum is too close to the cell body to work efficiently, because the presence of the cell body interferes with the induced velocity. For flagella much longer than the optimum length, the power required is much greater, but the flow rate increases only slightly as it approaches its limiting value. Thus, η^{-1} increases linearly with L/A for long flagella.

The final parameter to consider is the height of the cell body above the substrate. The flow rate as a function of H/A is shown in figure 12. The velocity is nearly constant for values of H/A greater than 10. When the height is less than this value, the velocity decreases slowly until $H/A = 5$, and then falls more rapidly. The effectiveness of a segment of the flagellum is determined by the ratio of its distance from the cell body to its distance from the substrate. For the shortest flagellum ($L/A = 5$), the flow rate decreases at a slower rate as H/A decreases, because all segments of the flagellum are proportionately closer to the cell body. Similarly, the velocity for $L/A = 10$ decreases more slowly than the velocity for $L/A = 20$. As a rough rule, it may be stated that the velocity changes negligibly when the height of the cell body is greater than the length of the flagellum.

The power consumption as a function of H/A is shown in figure 13. The actual power $\bar{P}$ changes very little over the range of H/A; hence the behaviour of η^{-1} is determined primarily by the flow rate. This means that η^{-1} increases rapidly when the height above the substrate is less than the length of the flagellum and shows negligible variation when the height is greater than the length of the flagellum.

To summarize the results for the body parameters, we find negligible change in the

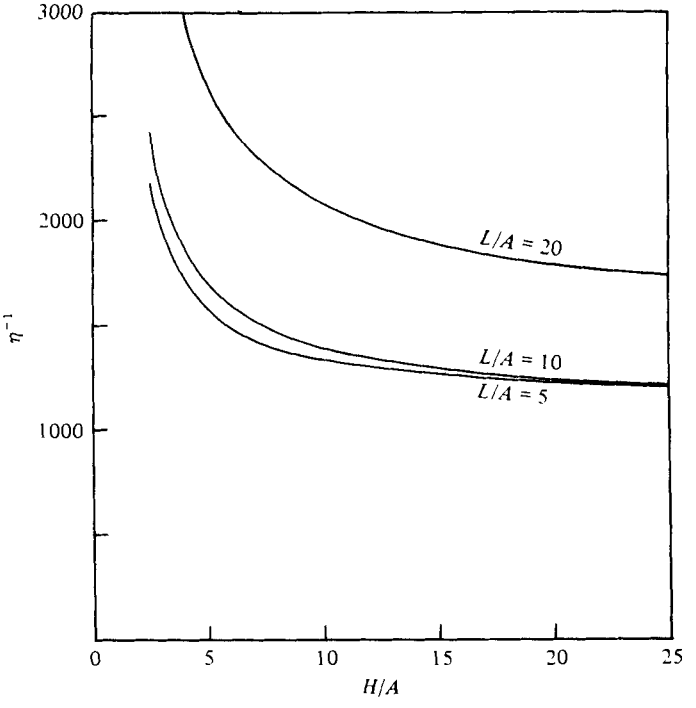

FIGURE 13. Power consumption as a function of height for three different length flagella with radius $a/A = 0{\cdot}02$. (Optimum values for wave parameters.)

power consumption η^{-1} as a function of a/A; hence there is no optimum flagellar radius. The optimum length of the flagellum is $L/A = 7$, with little change in the range $5 < L/A < 10$. There is no optimum height H/A, because the power consumption decreases monotonically with increasing height; however, η^{-1} shows negligible change when the height is greater than the length of the flagellum. Thus, $H = L$ may be taken as a lower limit for an efficient organism.

The preceding discussion has considered the dependence of the flow rate and power consumption on the parameters with the aim of determining the optimum values of the parameters. We now consider, in more detail, the flow generated by a single organism with dimensions and wave form approximating the optimal configuration. The organism has flagellar radius $a/A = 0{\cdot}02$, length $L/A = 10$ and height above the substrate $H/A = 10$. The wave consists of a single wavelength $N_\lambda = 1$, with $\alpha k = 2{\cdot}5$ and $k/k_E = 1$.

To examine the magnitude of the induced velocity, we consider the flow through the plane tangent to the cell body at the point of contact with the flagellum (which is parallel to the plane substrate). Figure 14 shows the velocity as a function of radial distance. The velocity shown is the average velocity around the edge of a disk of the specified radius, plotted at two points in the cycle and for the cycle average. The velocity increases rapidly with distance as the presence of the cell body becomes less important. It reaches a peak in the range $1{\cdot}5 < R/A < 2$, and then falls off inversely with radial distance. The peak velocity is reached at a distance approximately equal to the amplitude of the wave. There is a great variation in the magnitude of the

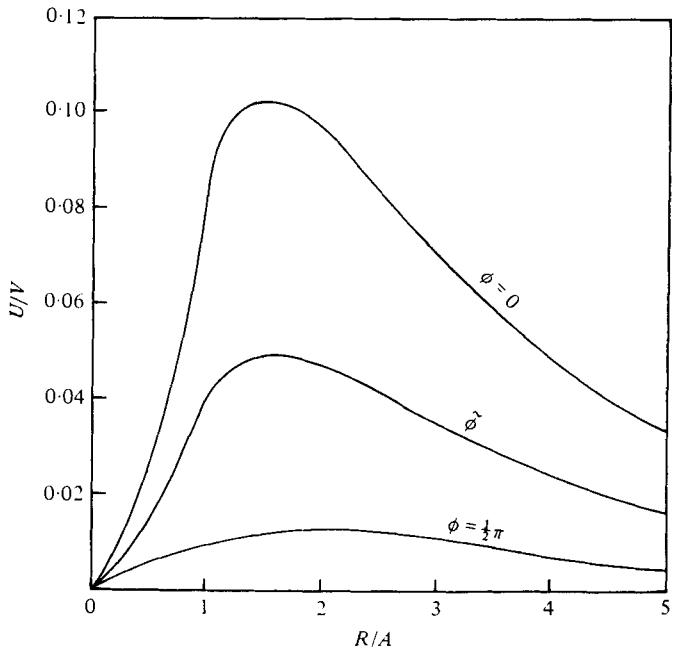

FIGURE 14. Instantaneous velocity as a function of radial distance for two points in the cycle and for the cycle average. (Flagellar length $L/A = 10$, radius $a/A = 0{\cdot}02$, height $H/A = 10$. Optimum values for wave parameters.)

velocity during the cycle. This effect is amplified by the fact that the velocity is evaluated at the base of the flagellum. If the velocity were evaluated over the surface of the collar, the flow would be more uniform over the cycle.

The major conclusion to be drawn from figure 14 is that the radius of the disk should be approximately equal to the amplitude of the wave. If the disk is smaller than this, it will be too close to the cell body to benefit from the full flow field. If it is much larger, it will extend into regions in which the velocity is much less than its peak value. This conclusion is the converse of the result that the optimum amplitude should equal the radius of the disk. It confirms this conclusion and shows the strong interdependence of these two parameters.

Finally, we look at a picture of the overall flow field in figure 15. Each line segment shows the direction of the time average velocity at that point. The magnitude of the velocity is inversely proportional to distance from the flagellum. Basically, each line segment shows the trajectory that a particle follows over the course of the cycle. Ideally, these lines should be drawn with their length proportional to the magnitude of the velocity; however, this would greatly reduce the clarity of the diagram. The segments close to the flagellum do not represent trajectories, because the velocity changes very rapidly as a function of both time and position.

We see that the fluid is drawn into the centre along the bottom, forced up past the organism and continues to move up and outward above the organism. At a height above the plane approximately level with the end of the flagellum and at a similar distance to each side of the organism is the centre of a large vortex. The fluid near the centre of each vortex remains at the centre over the course of several cycles. On

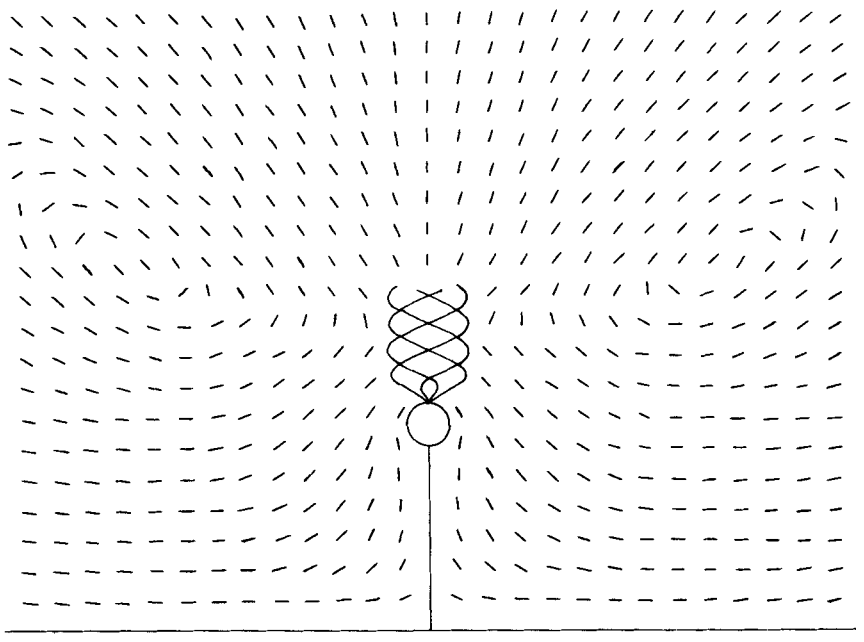

FIGURE 15. Flow diagram showing direction of particle motion. Wave propagates from base to tip. Flow is away from wall along central axis. Each line segment shows the direction of the time average velocity at that point. With the exception of points very close to the flagellum, the lines show the trajectories particles will follow.

the other hand, the cell body is in the centre of a stream which is constantly refreshed by fluid drawn in from infinity. This is essential for the feeding process to be successful.

10. Comparison with observations

The purpose of this study has not been to examine the detailed motion of any specific organism, but rather to determine the relative importance of the different parameters and, where possible, to find optimum values for the parameters. Nevertheless, the study would be incomplete without some comparison with observations of actual organisms.

As a particular case, we consider the choanoflagellate *Codonosiga*. This organism is one of the few choanoflagellates for which detailed information is available concerning the flagellar wave form and organism dimensions. The flagellar activity and fluid flow field for *Codonosiga* have been described by Lapage (1925) and Sleigh (1964).

In comparing the observations of *Codonosiga* with the results of this paper, we note two points on which the model and the actual organism differ. The first is the presence of hair-like appendages on the surface of the flagellum which are not considered in the model. Brennen (1976) studied the effect of surface hairs on the hydrodynamics of flagellar motion. He considered two distinct cases. For flagella with rigid surface hairs, the flow field is profoundly changed and the direction of flow is reversed compared with the flow produced by smooth flagella. For flagella with flexible hairs

which bend with the flow, Brennen concluded that the hydrodynamic effect was negligible. The surface hairs of *Codonosiga* are of this second type, hence they are ignored.

The second point on which the model and the organism differ concerns the flagellar wave form. The organism employs a non-sinusoidal wave which might be more accurately represented by arcs and lines. The variation of the parameter k/k_E in figures 6 and 7 shows the changes in flow velocity and power consumption which may be expected in going from a sine wave to a more general wave of similar shape. We conclude that the changes are insignificant in determining optimal parameter values, but may be significant if accurate values of the flow velocity and power consumption are required. Thus, we may compare the predicted optima with the observations by using the parameters of the sine wave which most closely approximates the actual wave.

To compare the values of the parameters, we consult Sleigh to obtain approximate dimensions: $A = 5\,\mu$m, $L = 25$–$30\,\mu$m, $\lambda = 15$–$20\,\mu$m, $H = 20$–$100\,\mu$m. From the tracing of the wave form, approximate values for N_λ and αk are: $N_\lambda = 1$–$1{\cdot}5$ and $\alpha k = 2$. If we compare these dimensions with the predicted optima, we find that the observations are generally consistent with predictions. In particular, the observed value $L/A = 5$–6 agrees with the predicted optimum range $5 < L/A < 10$. The observed height gives $H/L = 0{\cdot}7$–4, compared with the prediction that the minimum height should be approximately equal to the flagellar length. The observed wave parameters N_λ and k show excellent agreement with the predicted optima, $N_\lambda = 1$ and $2 < \alpha k < 2{\cdot}5$ for this length flagellum.

An additional comparison of the model and the observations can be made by examining the flow field. The qualitative description of the flow field given by Sleigh and the schematic diagram shown by Lapage closely resemble the calculated flow field shown in figure 15. This confirms the validity of the assumptions made in comparing the results of the model with the observations of *Codonosiga*.

The comparisons made in this section support the predictions made in § 9 and demonstrate the value of this model in studying organisms such as *Codonosiga*. We emphasize that the model is not restricted to sinusoidal waves, and that any wave form may be considered, whether it is expressed analytically or numerically.

I wish to thank Professor M. J. Lighthill for his helpful comments and suggestions. I acknowledge the support of the National Science Foundation through the Graduate Fellowship Program.

Appendix. Computing

The numerical procedures used in this paper divide the flagellum into N segments. All segments were of equal length with the exception of the segments at the ends, which were chosen to be not less than twice the diameter of the flagellum. All calculations were performed using IBM 370 double precision to avoid errors in dealing with large numbers whose difference is very small. The large matrices were stored as single precision to save storage space.

The iteration procedure converged with an error of less than 1% after four iterations. The iteration was carried further to ascertain that this was a true convergence.

The number of segments required varied according to the values of the wave parameters; but, for a typical case, 20 segments per wavelength produces an error of less than 1%.

The equations were solved at four points in the half cycle of the wave to determine the flow rate and power consumption with an error of less than 1%.

For a wave with the flagellum divided into 40 segments, the calculations for the complete cycle required approximately 20 s of IBM 370 CPU time.

To test the accuracy of the image systems, the velocity was evaluated at several points on the boundaries. The exact expression for the Green's function was compared to its far-field expansion, and the Cartesian expression was checked against the simpler result for the radial component.

To test the accuracy of the solution, the calculated velocity was compared with the velocity of the flagellum at points along the flagellum. Comparisons were made with asymptotic results based on force coefficients.

REFERENCES

BLAKE, J. R. 1971 *Proc. Cam. Phil. Soc.* **70**, 303.

BRENNEN, C. 1976 *J. Mechanochem. Cell. Motil.* **3**, 207.

HIGDON, J. J. L. 1979 *J. Fluid Mech.* **90**, 685.

LAPAGE, G. 1925 *Quart. J. Micro. Sci.* **69**, 471.

LIGHTHILL, M. J. 1976 *SIAM Reviews* **18**, 161.

LUNEC, J. 1975 In *Swimming and Flying in Nature* (ed. T. Y. Wu, C. J. Brokaw & C. Brennen). New York: Plenum.

OSEEN, C. W. 1927 *Hydrodynamik*. Leipzig: Akad. Verlag.

SLEIGH, M. A. 1964 *Quart. J. Micro. Sci.* **105**, 405.

SLEIGH, M. A. 1973 *The Biology of Protozoa*. London: Arnold.